



Temporal and Spatial Local Scour Profile of Cylindrical Pier in Cohesive Sediment Mixture

Mojtaba Porhemmat¹ · Zohreh Sheikh Khozani² · Wan Hanna Melini Wan Mohtar¹  · Siti Fatin Mohd Razali¹ · Ahmed El-Shafie³

Received: 25 April 2023 / Accepted: 8 April 2024 / Published online: 2 May 2024
© The Author(s), under exclusive licence to Shiraz University 2024

Abstract

Local scour estimation in bridge piers is one of the main elements to design new bridges and to monitor existing bridges. It is important to obtain the maximum local scour depth in designing the level of foundation or countermeasures for the existing bridges. In this experimental study, an attempt was made to investigate the effect of cohesion on temporal and spatial local scour around cylindrical bridge pier in sand-clay sediment mixture. Two sizes of sands (with median grain size $D_{50}=0.59$ mm and 0.99 mm) with different percentages of cohesive materials (0–30%) were used. The cohesive material contains 90% kaolinite and 10% bentonite. The results show that the location of maximum scour depth y_{sumax} varied for different time intervals based on the percentage of clay. Upstream side scouring dominates the scouring process at early stages before propagates to the upstream of pier for low flow velocity and low percentage of clay. Increasing flow velocity and clay percentage gives significant downstream side scouring throughout the experiments. The percentage of clay in the sediment mixture does not necessarily influence the maximum ultimate value of scour depth. The maximum ultimate scour depth was occurred at the upstream, usually at the pier nose, while the minimum ultimate scour depth was observed to occur at the downstream for the sand-clay sediment mixtures with up to 20% of cohesive materials. However, an adverse profile was observed for the sediment mixture with 30% of cohesive material where the maximum scour depth occurred at the downstream.

Keywords Temporal and spatial scour profile · Sand-clay bed material · Cylindrical pier

1 Introduction

Bridges have been a big challenge for engineers in design, operation and maintenance stages due to the complexity of hydraulic and structural designs. Hydraulic structures such as bridges in the rivers can disturb the flow characteristics and induce the force interaction between the structure and the natural flow. Such obstacles change the flow pattern when the flow approaches the structure, modifying the flow condition and increasing the turbulence intensity around the pier, which subsequently provide a strong erosive power for the local streamflow. The changes of flow around bridge pier include the formation of downflow (like a vertical jet), horseshoe vortex (due to the formation of scour hole), and wake vortex (due to the boundary layer separation). Therefore, such an erosive power endangers the stability of bridge foundation and can cause bridge failures (Brandimarte et al. 2012).

The detailed research on scour related hydraulic issues is important not only for minimizing bridge failure, but also

✉ Wan Hanna Melini Wan Mohtar
hanna@ukm.edu.my

Mojtaba Porhemmat
mojtaba@ukm.edu.my

Zohreh Sheikh Khozani
y.sheikh@gmail.com

Siti Fatin Mohd Razali
fatinrazali@ukm.edu.my

Ahmed El-Shafie
elshafie@um.edu.my

¹ Department of Civil Engineering, Faculty of Engineering and Built Environment, Universiti Kebangsaan Malaysia (UKM), 43600 Bangi, Selangor, Malaysia

² Institute of Structural Mechanics, Bauhaus Universität Weimar, 99423 Weimar, Germany

³ Department of Civil Engineering, Faculty of Engineering, Universiti Malaya, Kuala Lumpur, Malaysia

the costs for bridge construction can be reduced by 40% if the accurate scour depth can be estimated (Dumas and Krolack 2002). In this light, numerous empirical equations are developed to predict the maximum scour depth for a specific bridge design and hydraulic condition, with notably the HEC-18 (also known as the Colorado State University), and Florida Dot formulae (Arneson et al. 2012), integrating the important criteria of hydraulics, sediment and the pier characteristics. However, the previous studies related to local scour, mainly focused on the investigation of maximum scour depth around the bridge pier on cohesionless materials, for example, sand and gravel (Akib et al. 2011; Mazumder 2017). The complexity of cohesive bed material, involving chemical and physical bonding of the colloid clay particles present a different scour profile when calculated using cohesion-less sediment-based equations. The entrainment of cohesive bed material into the outer layer requires forces to exceed two-inter particular forces, i.e., gravity and cohesive (electrochemical) force (Link et al. 2013; Devi and Barbhuiya 2017).

Numerous experimental and numerical studies were utilized in different conditions (clear-water with uniform bed sediment or cohesive bed) to estimate the scour depth and empirical equations were derived (Dey and Barbhuiya 2004; Najafzadeh and Lim 2015; Hosseinjanzadeh et al. 2019; Namaee and Sui 2019; Singh et al. 2020; Yang et al. 2020; Khosravi et al. 2021). For a combination of clay-sand cohesive sediment layers, Chaudhuri et al. (2018) presented a set of new data on local scour in protracted contraction. They proposed some empirical equations to calculate scour depth around square and circular pier shapes and found that with increasing the mean velocity maximum equilibrium of scour depth around piers were increased. Das et al (2020) studied on the effect of pier shapes and sizes on scouring process experimentally. They investigated on fine sand and silt beds and found that these two parameters shape and size of piers made significantly changes on scouring process. An experimental setup was conducted to investigate the temporal variation of scour depth in cohesionless and cohesive sediment by Ansari et al. (2002). They applied the method of Kothyari et al., (1992) for cohesionless sediment to develop a mathematical model to calculate the temporal variation of scour depth.

It is known that the local scour experiments require a long period of time for cohesionless sediment, thus it is expected similar time frame if not longer for cohesive sediment. Although a longer experimental time guarantees an accurate representation of equilibrium maximum scour depth, it is neither cost effective nor practical to conduct an experiment at such long hours. However, the data obtained from a short experimental period of 10–12 h could be less than 50% of the equilibrium scour depth (Melville and Chiew 1999). Based on this, the scour depth obtained in shorter

experimental period multiplied by a factor to get the actual equilibrium scour depth. Even so, the spatial profiles differ particularly in terms of the transversal and downstream scour lengths. As such, it is necessary and crucial to run an experiment for longer time in order to obtain a holistic scouring description. Special and expensive tools are required to measure temporal and spatial scouring, which is more crucial in cohesive bed, and the measurement process is time consuming. Furthermore, due to long hours of experimental runs, a temporal uniform and systematic measurement is restricted without automated instruments.

Scour at bridge piers in clay (i.e., cohesive sediment) or in sand-clay mixture (that is a non-cohesive and cohesive sediment mixture) have scarcely investigated. The plausible reason is attributed to the complexity in the mechanisms of scour in clay bed, due to the effects of electromagnetic and electrostatic inter-particle forces, leading to the experimental difficulties (Partheniades 2009; Link et al. 2013). Even so, studies such as Debnath and Chaudhuri (2010, 2011) have conducted experiments on local scour around varying bridge pier shapes for cohesive/sand mixtures with fractions of cohesive material varying from 35 to 100%, and provide insights on how the scour profiles are for such sediment mixture.

The work of both Debnath and Chaudhuri focused on the fine sand (diameter of 0.182 mm) with kaolinite clay. The main objectives of these studies are to investigate the effect of cohesion on temporal and spatial local scour around cylindrical bridge pier in coarse sand-clay sediment mixture under varying flow characteristics. The presence of clay in a sediment mixture plays an important role by significantly reduced the scour depths and the scouring area. Clay also changes the scouring process development whereby the commencement of scouring and the maximum of scouring depth was found at the sides of pier, differed for sand mixtures with both locations were at the front of a pier. The movement of sediment was reported to be different where the scouring process in was particle-by-particle in sand bed, compared to the aggregate by aggregate or a form of chunks for cohesive sediment mixture.

This paper dwells into more detailed temporal and spatial scouring development for cohesive sediment mixture, taking into account the peripheral scouring profiles and areas, based on coarser sand-clay sediment mixture. We investigate the interaction of sediment movement and the influence of cohesive behaviour in a sand-cohesive sediment mixture (with bigger sand size of 0.59 mm and 0.99 mm), complementing and adding crucial information to the Diab and Chaudhari's work. The layout for this paper starts with the description of detailed methodology of experimental setup, including the sediment distribution of cohesive material/sand and measurement of spatial and temporal scour depth. Then, the evolution of the peripheral scour depth and profile around the

bridge pier for each varying percentage of cohesive material is presented in the analysis and discussion sections.

2 Methodology and Flume Setup

2.1 Experimental Facility

All the experiments for this research were conducted in the coastal laboratory of the Universiti Kebangsaan Malaysia (UKM). The experiments were conducted in a recirculating tilting flume, 8 m long, 1 m wide and 1 m deep, where the slope was kept constant at 0.001 as illustrated in Fig. 1a. The flume side walls were made from transparent Perspex to permit visual observation and monitoring.

The submersible pump was installed in the circulation tank. The bypass pipe was fixed after the pump to control the discharge in the flume. The extra discharge led to the circulation tank by bypass pipe equipped with a valve. The floating valve was used to keep a constant water depth in the circulation tank. The high discharge in the flume inlet pipe causes high vorticity and turbulence in the inlet tank. The flow straightener was made from PVC pipe with 26.67 mm outside diameter and 30 cm length, stacked and fixed at the flume entrance to reduce the turbulence and vorticity intensities from the inlet tank into the flume as seen in Fig. 1. The flow straightener dampens the turbulence and straightens the flow. Figure 1a illustrates the visual presentation of the experimental setup.

A water resistant with 0.1 m diameter as full scaled transparent Perspex made cylindrical pier was fixed in the middle of the test section (about 6 m from the inlet). Since Perspex is waterproof, it protects the electrical instrument within the pier, whereby camera was used as the measurement device. The pier diameter is designed 0.1 m ($w/D=0.1$) to avoid the sidewall effect as suggested by Chiew (1984).

The symbol w and D denote as the flume width and pier diameter, respectively.

2.2 Experimental Condition

The flow velocity was monitored using Nortek ADV velocimeter (with measurement taken using frequency of 100 Hz), installed on a self-made ADV_{XYZ} electrical traverse (Fig. 1). The velocity was varied from 22 to 42 cm/s, and the flow depth (y) was kept constant at 30 cm (that is 3 times of the pier diameter D) to avoid the flow depth effect suggested by Melville (1975). The chosen ratio (y/D) ensured that the local scour is in narrow pier condition. The flow velocity was obtained by measuring the depth average velocity at $0.2y$ and $0.8y$ and by averaging them, as it had been done in some similar previous studies (Ting et al. 2001; Debnath and Chaudhuri 2011), where y is the depth of water. Recall that to maintain a uniform flow during each experiment, the 17 cm depth false floor was constructed at both upstream and downstream of the working area. Also, the discharge and the flow depth were kept constant during each experiment to ensure a uniform flow is obtained throughout. The height of flume makes it difficult and slows down the process of adjusting the ADV in the desired location using the manual traverse. The experiments are designed with different percentages of cohesive mixture (C_p) and different velocities. A total of 27 experiments were conducted with various sand size, clay percentage and flow Reynolds number Re as shown in Table 1. The Reynolds number is calculated as $Re = \frac{\rho VR}{\mu}$, where ρ is water density, R is hydraulic radius ($R = A/P$), A is flow area, P is wetted perimeter and μ is the water viscosity. The experiments are categorized in based on the type of sediment as A and B, with the first number indicate percentage of clay, and the last number indicate the run

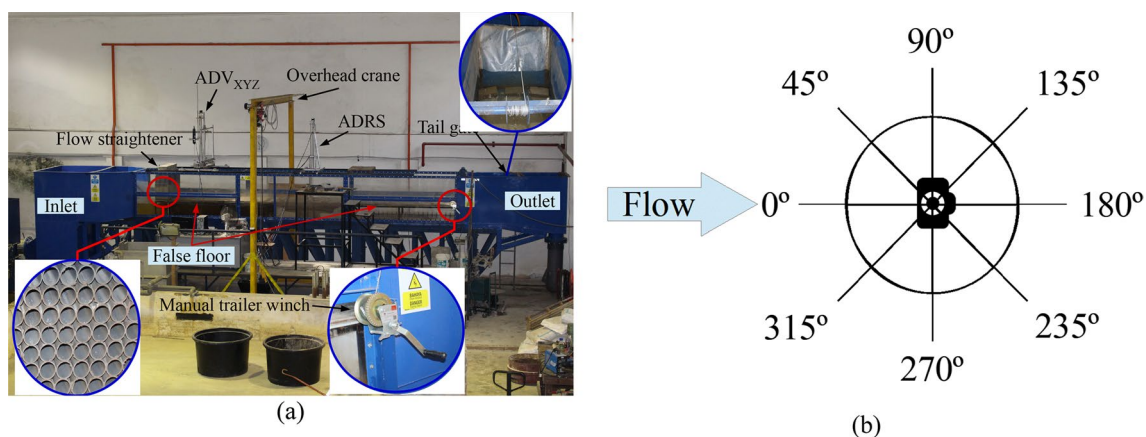


Fig. 1 a Visual display of flume used for the experiments and b the schematic diagram of the position of the camera inside the pier

Table 1 The range of experimental conditions

| Row | Run | D_{50} (mm) | C_p (%) | V (cm/s) | y (cm) | Re | Fr | Re_{pi} |
|-----|------|---------------|-----------|------------|----------|--------|-------|-----------|
| 1 | A001 | 0.59 | 0 | 22 | 30 | 36,184 | 0.128 | 22,000 |
| 2 | A002 | 0.59 | 0 | 24 | 30 | 39,474 | 0.14 | 24,000 |
| 3 | A003 | 0.59 | 0 | 28 | 30 | 46,053 | 0.163 | 28,000 |
| 4 | A004 | 0.59 | 0 | 32 | 30 | 52,630 | 0.186 | 32,000 |
| 5 | A101 | 0.59 | 10 | 28 | 30 | 46,053 | 0.163 | 28,000 |
| 6 | A102 | 0.59 | 10 | 32 | 30 | 52,630 | 0.186 | 32,000 |
| 7 | A103 | 0.59 | 10 | 36 | 30 | 59,868 | 0.21 | 36,000 |
| 8 | A104 | 0.59 | 10 | 42 | 30 | 69,079 | 0.245 | 42,000 |
| 9 | A201 | 0.59 | 20 | 28 | 30 | 46,053 | 0.186 | 32,000 |
| 10 | A202 | 0.59 | 20 | 32 | 30 | 52,630 | 0.21 | 36,000 |
| 11 | A203 | 0.59 | 20 | 36 | 30 | 59,868 | 0.245 | 42,000 |
| 12 | A204 | 0.59 | 20 | 42 | 30 | 69,079 | 0.245 | 42,000 |
| 13 | A301 | 0.59 | 30 | 36 | 30 | 59,868 | 0.21 | 36,000 |
| 14 | A302 | 0.59 | 30 | 42 | 30 | 69,079 | 0.245 | 42,000 |
| 15 | B001 | 0.99 | 0 | 22 | 30 | 36,184 | 0.128 | 22,000 |
| 16 | B002 | 0.99 | 0 | 24 | 30 | 39,474 | 0.14 | 24,000 |
| 17 | B003 | 0.99 | 0 | 28 | 30 | 46,053 | 0.163 | 28,000 |
| 18 | B004 | 0.99 | 0 | 32 | 30 | 52,630 | 0.186 | 32,000 |
| 19 | B101 | 0.99 | 10 | 32 | 30 | 52,630 | 0.186 | 32,000 |
| 20 | B102 | 0.99 | 10 | 36 | 30 | 59,868 | 0.21 | 36,000 |
| 21 | B103 | 0.99 | 10 | 42 | 30 | 69,079 | 0.245 | 42,000 |
| 22 | B201 | 0.99 | 20 | 28 | 30 | 46,053 | 0.163 | 28,000 |
| 23 | B202 | 0.99 | 20 | 32 | 30 | 52,630 | 0.186 | 32,000 |
| 24 | B203 | 0.99 | 20 | 36 | 30 | 59,868 | 0.21 | 36,000 |
| 25 | B204 | 0.99 | 20 | 42 | 30 | 69,079 | 0.245 | 42,000 |
| 26 | B301 | 0.99 | 30 | 36 | 30 | 59,868 | 0.21 | 36,000 |
| 27 | B302 | 0.99 | 30 | 42 | 30 | 69,079 | 0.245 | 42,000 |

number (with varying Re). Each run is given name as shown in the 2nd column of Table 1, where for example A102 denotes experiment using sand A, 10% of clay fraction and 02 is experiment no 2 for the same sediment mixture. The pier Reynolds number Re_{pi} is calculated as $Re_{pi} = \frac{\rho V D}{\mu}$. The cohesive sediment added to sand A and B with different percentages of 0%, 10%, 20% and 30%.

During all experiments the flow depth, pier shape and pier diameter were maintained as constant, which means that the only variable that influences on the flow characteristics (for example the Reynolds number or pier) is the flow velocity. The Hjulstrom curve (1935) was used to determine the critical velocity for cohesionless sands. To find the critical velocity for cohesive sands, the method used by Porhemmat et al. (2016) was applied, giving the critical velocity (V_c) are 28 cm/s and 32 cm/s for sand A and sand B, respectively.

The clay-sand mixture was freshly prepared for each experimental setup by mixing homogeneously the cohesive material with the sand based on the percentages given in Table 2. The bed was prepared by pouring the sediment

mixtures in layers until 25 cm, manually compacting with the same weight and levelled with the false floor using a trowel. The water was slowly filled in not to disturb the prepared bed until reaching a water depth of 0.2 m, before filling the flume up to the desired approach flow depth (based on the desired discharge). The development of scouring process was assessed based on images taken at azimuthal view (0° – 360° , with 45° interval) at each hour until experiment ends.

A low-cost automated data recording system (ADRS) controlled by Arduino microcontroller was designed and developed to obtain spatial and temporal data in different time intervals. The comparison between manual measurements and the ADRS confirmed that it is capable of recording data with high accuracy and the ADRS is able to provide a holistic view of both peripheral spatial and temporal variability in the development of local scour around bridge piers on a laboratory scale.

Each experiment was ended when the scour rate becomes less than D_{50} /hour (similar to the time suggested by Link et al. (2008)). Once the experiment ended, the flow was gradually decreased (by lowering the tail gate), with extra care

Table 2 Summary of temporal and ultimate experimental data of local scour for cohesionless and cohesive sands

| Row | Run | D_{50} (mm) | V (cm/s) | $\frac{V}{V_c}$ | Re_{pi} (K) | y_{sumth} (cm) | α° | y_{sumth} (cm) | α° | $\frac{y_{sumth}}{y_{sumax}}$ | α° | $\frac{y_{sumth}}{y_{sumax}}$ | α° | L_u (cm) | $\frac{L_u}{y_{sumax}}$ | L_s (cm) | $\frac{L_s}{y_{sumax}}$ | $\frac{L_u}{L_s}$ |
|-----|------|---------------|------------|-----------------|---------------|------------------|----------------|------------------|----------------|-------------------------------|----------------|-------------------------------|----------------|------------|-------------------------|------------|-------------------------|-------------------|
| 1 | A001 | 0.59 | 22 | 0.79 | 22 | 8 | 0 | 4.2 | 180 | 0.53 | 53 | 0.08 | 180 | 12 | 1.50 | 12 | 1.50 | 1.00 |
| 2 | A002 | 0.59 | 24 | 0.86 | 24 | 13.7 | 0 | 9 | 180 | 0.66 | 51 | 0.18 | 180 | 20 | 1.46 | 24 | 1.75 | 0.83 |
| 3 | A003 | 0.59 | 28 | 1.00 | 28 | 17.1 | 0 | 13.2 | 180 | 0.77 | 51 | 0.24 | 180 | 26 | 1.52 | 30 | 1.75 | 0.87 |
| 4 | A004 | 0.59 | 32 | 1.14 | 32 | 18 | 0 | 13.9 | 180 | 0.77 | 59 | 0.32 | 180 | 26 | 1.44 | 30 | 1.67 | 0.87 |
| 5 | B001 | 0.99 | 22 | 0.69 | 22 | 4.7 | 45 | 1.7 | 180 | 0.36 | 50 | -0.21 | 180 | 6 | 1.28 | 6 | 1.28 | 1.00 |
| 6 | B002 | 0.99 | 24 | 0.75 | 24 | 7.7 | 0 | 4.6 | 180 | 0.60 | 57 | 0.06 | 180 | 12 | 1.56 | 12 | 1.56 | 1.00 |
| 7 | B003 | 0.99 | 28 | 0.88 | 28 | 14.3 | 0 | 9.3 | 180 | 0.65 | 45 | 0.11 | 180 | 20 | 1.40 | 24 | 1.68 | 0.83 |
| 8 | B004 | 0.99 | 32 | 1.00 | 32 | 17.3 | 0 | 12.6 | 180 | 0.73 | 50 | 0.19 | 180 | 22 | 1.27 | 30 | 1.73 | 0.73 |
| 9 | A101 | 0.59 | 28 | 0.78 | 28 | 13.05 | 45 | 10.2 | 180 | 0.78 | 53 | 0.28 | 180 | 18 | 1.38 | 22 | 1.69 | 0.82 |
| 10 | A102 | 0.59 | 32 | 0.89 | 32 | 15.3 | 0 | 11 | 180 | 0.72 | 51 | 0.27 | 180 | 22 | 1.44 | 24 | 1.57 | 0.92 |
| 11 | A103 | 0.59 | 36 | 1.00 | 36 | 17.4 | 0 | 12.4 | 180 | 0.71 | 64 | 0.50 | 0 | 24 | 1.38 | 28 | 1.61 | 0.86 |
| 12 | A104 | 0.59 | 42 | 1.17 | 42 | 18.5 | 0 | 14 | 180 | 0.76 | 69 | 0.48 | 180 | - | - | - | - | - |
| 13 | B101 | 0.99 | 32 | 0.86 | 32 | 10.5 | 90 | 7.3 | 180 | 0.70 | 57 | 0.19 | 180 | 14 | 1.33 | 16 | 1.52 | 0.88 |
| 14 | B102 | 0.99 | 36 | 0.97 | 36 | 14.8 | 0 | 10 | 180 | 0.68 | 61 | 0.24 | 180 | 22 | 1.49 | 22 | 1.49 | 1.00 |
| 15 | B103 | 0.99 | 42 | 1.14 | 42 | 17.7 | 0 | 13.3 | 180 | 0.75 | 65 | 0.37 | 180 | 24 | 1.36 | 26 | 1.47 | 0.92 |
| 16 | A201 | 0.59 | 28 | 0.67 | 28 | 7.4 | 90 | 3.5 | 0 | 0.47 | 72 | 0.27 | 0 | 7.5 | 1.01 | 12.5 | 1.69 | 0.60 |
| 17 | A202 | 0.59 | 32 | 0.76 | 32 | 11.1 | 0 | 9.2 | 180 | 0.83 | 71 | 0.51 | 180 | 12 | 1.08 | 16 | 1.44 | 0.75 |
| 18 | A203 | 0.59 | 36 | 0.86 | 36 | 16.1 | 45 | 11.8 | 180 | 0.73 | 33 | 0.20 | 180 | 16 | 0.99 | 20 | 1.24 | 0.80 |
| 19 | A204 | 0.59 | 42 | 1.00 | 42 | 17.8 | 0 | 14 | 135 | 0.79 | 53 | 0.28 | 180 | 22 | 1.24 | 26 | 1.46 | 0.85 |
| 20 | B201 | 0.99 | 28 | 0.67 | 28 | 10.8 | 0 | 9 | 45 | 0.83 | 44 | 0.24 | 180 | 12 | 1.11 | 16 | 1.48 | 0.75 |
| 21 | B202 | 0.99 | 32 | 0.76 | 32 | 13.7 | 0 | 9 | 180 | 0.66 | 52 | 0.33 | 180 | 16 | 1.17 | 22 | 1.61 | 0.73 |
| 22 | B203 | 0.99 | 36 | 0.86 | 36 | 16.5 | 0 | 11 | 180 | 0.67 | 39 | 0.30 | 0 | 16 | 0.97 | 24 | 1.45 | 0.67 |
| 23 | B204 | 0.99 | 42 | 1.00 | 42 | 17.8 | 0 | 13 | 180 | 0.73 | 51 | 0.39 | 180 | 20 | 1.12 | 26 | 1.46 | 0.77 |
| 24 | A301 | 0.59 | 36 | 0.73 | 36 | 9.8 | 135 | 2.1 | 0 | 0.21 | 26 | 0.00 | 0 | 12 | 1.22 | 14 | 1.43 | 0.86 |
| 25 | A302 | 0.59 | 42 | 0.86 | 42 | 12.9 | 90 | 11.7 | 0 | 0.91 | 28 | 0.18 | 180 | 20 | 1.55 | 22 | 1.71 | 0.91 |
| 26 | B301 | 0.99 | 36 | 0.73 | 36 | 7.6 | 135 | 1.5 | 0 | 0.20 | 57 | 0.13 | 0 | 4 | 0.53 | 8 | 1.05 | 0.50 |
| 27 | B302 | 0.99 | 42 | 0.86 | 42 | 7.9 | 180 | 1.8 | 0 | 0.23 | 82 | 0.23 | 0 | 10 | 1.27 | 10 | 1.27 | 1.00 |

is given one the water depth reached 5–10 cm not to disrupt the developed scour hole. The contained water in the scour hole was carefully siphoned out using a tube. The detailed geometry of the scour hole was systematically measured in grid of $1\text{ cm} \times 1\text{ cm}$ using a laser distance meter.

Each image taken at different angles throughout the experimental runs were analysed, giving the temporal and spatial development of local scour and the ultimate condition for each experiment. Note that in this study, y_{su} stands for scour depth at ultimate condition for each experiment, while y_{se} stands for the maximum scour depth at the equilibrium condition when $V/V_c = 1$.

3 Results

The discussion starts with the findings based on the cohesionless sand experiments followed by analysis from the clay-sand mixtures. As the obtained scour hole has symmetrical pattern along the horizontal lines, the maximum scour depth y_{sumax} and scouring rate were described for angles at

0° , 45° , 90° , 135° and 180° only, representing the upstream, side, and downstream of the pier, as shown in Fig. 1b.

3.1 Scour Depth for Cohesionless Sands

Two series of experiments (Series A00 and Series B00) were conducted for cohesionless sands. The temporal development $T = \frac{Vt}{a}$ of local scour with varying Re_{pi} at different acquisition angles next to the pier perimeter, obtained from the photos taken by ADRS, is shown in Fig. 2.

There was a high rate of aggradation at the downstream of the pier perimeter, which causes low scour rate at downstream (sometimes almost no scour, for example at $t = 5, 6, 7$ and 8 h as can be seen in Fig. 2. For illustration purposes, only experiments at low and high velocities were presented. It is believed that this high aggradation is due to low V/V_c as the sediment settles back to the bed when the turbulence intensity can no longer sustain them in suspension. The temporal development of scour had almost similar profile in all upstream locations, i.e., at $\alpha = 0^\circ, 45^\circ$ and 90° . The same profiles were observed as well for the temporal development for downstream locations, i.e., $\alpha = 135^\circ$ and 180° .

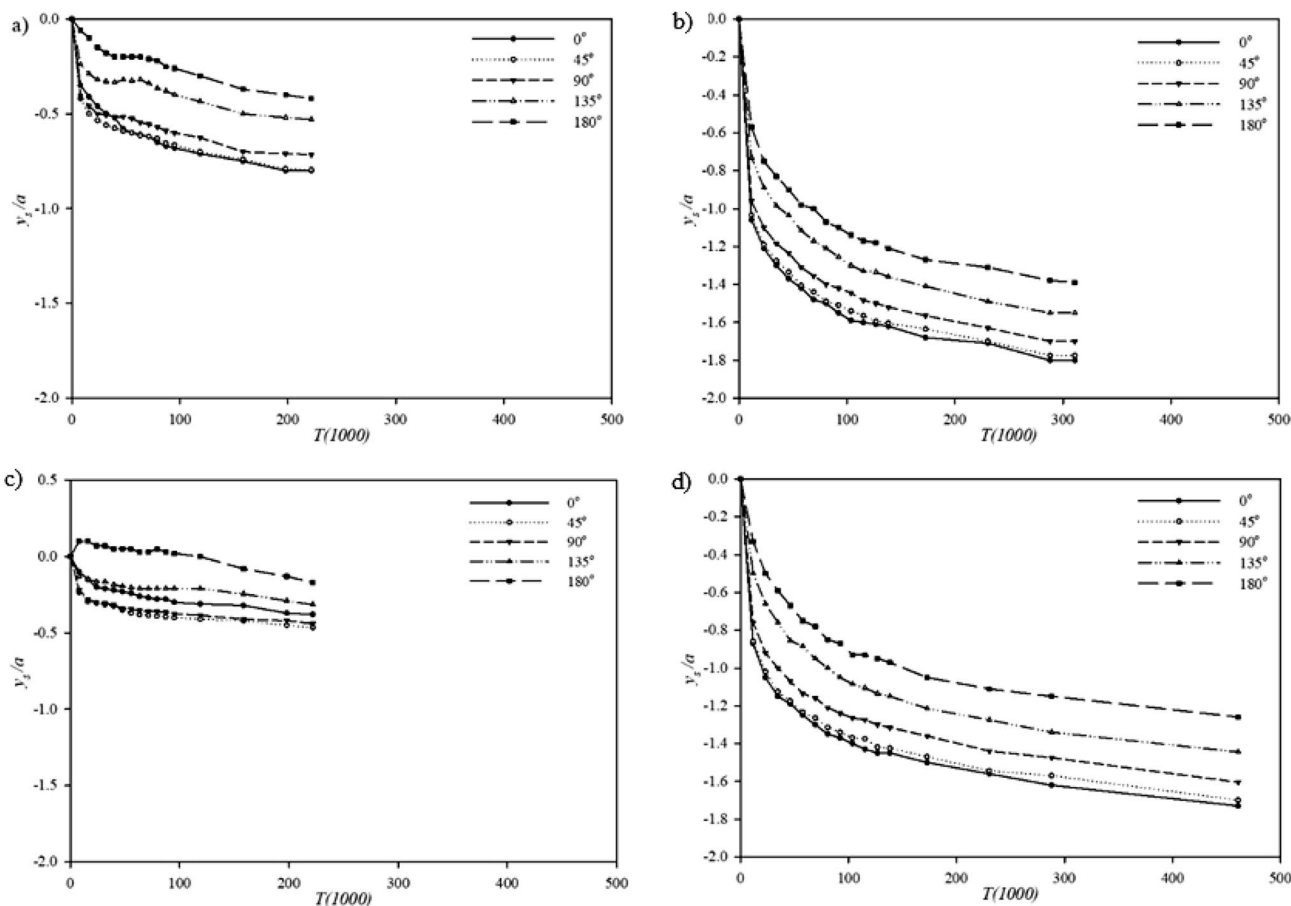


Fig. 2 Temporal scour depth around the pier for cohesionless sand **a** Run A001, **d** Run A004, **e** Run B001, **h** Run B004 at varying α

For all Reynolds numbers, the maximum ultimate scour depth was consistently located at the upstream of pier at $\alpha = 0^\circ$. Data shows that the maximum scour and scour rate produced nearly similar profiles at $\alpha = 0^\circ$ and $\alpha = 45^\circ$. Throughout the experiments, the minimum scour depth y_{smin} was consistently found at $\alpha = 180^\circ$. Although, the maximum ultimate scour depth for $V/V_c = 1$ and 1.14 had almost the same value but the scour rate had higher value when $V/V_c = 1.14$. In the first hour of experiment the highest scour rates were found 87 mm/h, and 106 mm/h at $V/V_c = 1$ and 1.14, respectively, whereas the minimum scour rates were 41 mm/h and 57 mm/h.

Beside to the temporal peripheral scour depth, the spatial characteristics of the ultimate scour hole is also investigated

in this study. The ultimate upstream length of scour hole is defined as L_u and the side length is defined as L_s . The left and right side of the scour hole shows a nearly symmetrical shape. The side length of pier (L_s) was obtained based on one half-side and is the representative of the other half due to symmetrical scour geometry.

Figure 3 depicts the spatial diagram of ultimate scour hole for sand A with different pier Reynolds numbers. According to the results of Fig. 5 with increasing the Re_{pi} , the upstream length increased (from 12 cm for Run A001 to 26 cm for Run A003) and the side lengths became wider (from 14 cm for Run A001 to 30 cm for Run A003). Interestingly, the upstream and the side length values at Run A003 were similar to the values of Run A004, which were, $L_u = 1.44 y_{smax}$

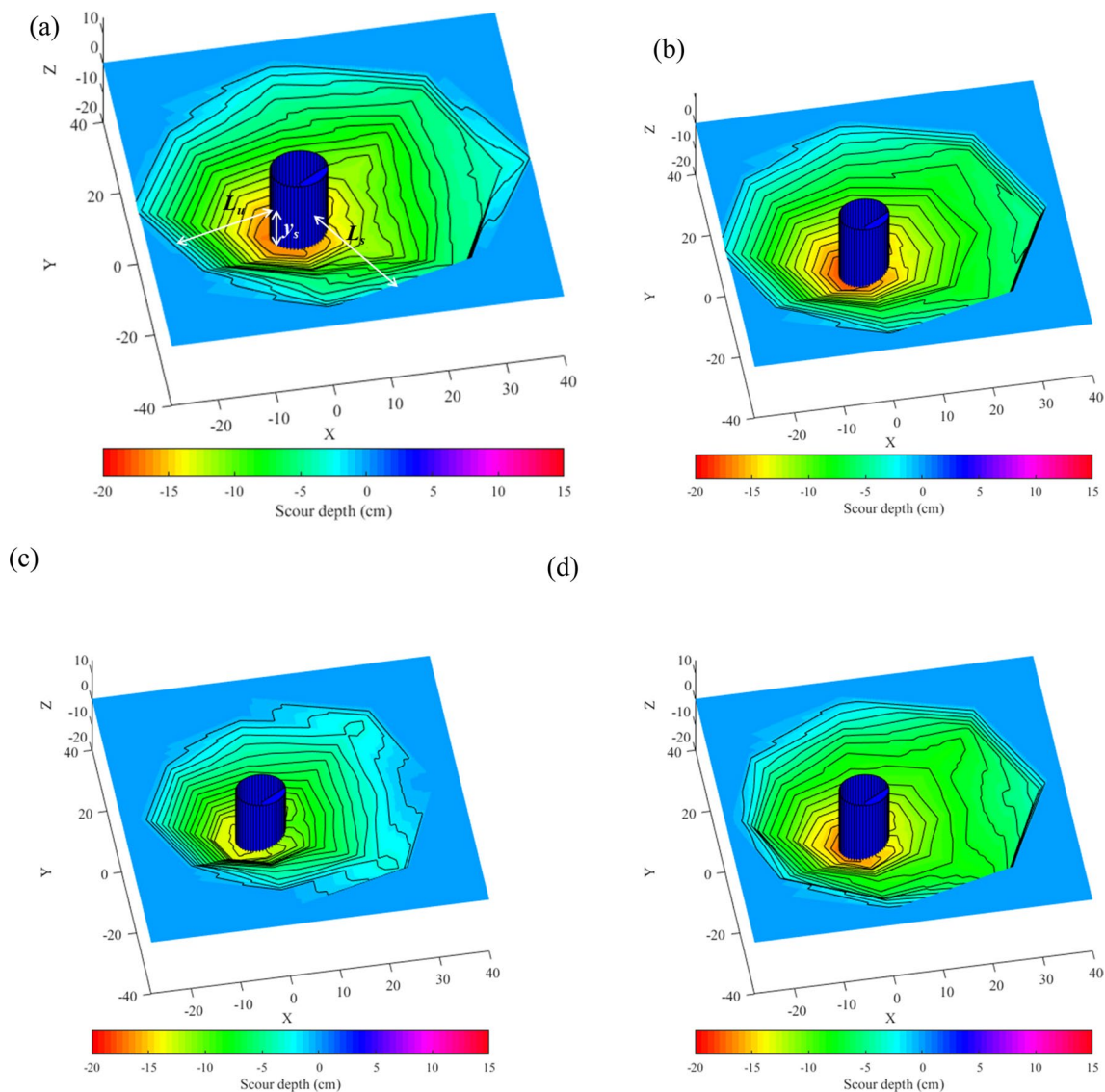


Fig. 3 The spatial characteristics of developed scour hole for sand A with no added cohesive material. Plots shown are: **a** Run A001, $Re_{pi} = 22$ K, **b** Run A002, $Re_{pi} = 24$ K, **c** Run A003, $Re_{pi} = 28$ K, **d** Run A004, $Re_{pi} = 32$ K. For a graphical description of L_u , L_s and y_s , refer to a

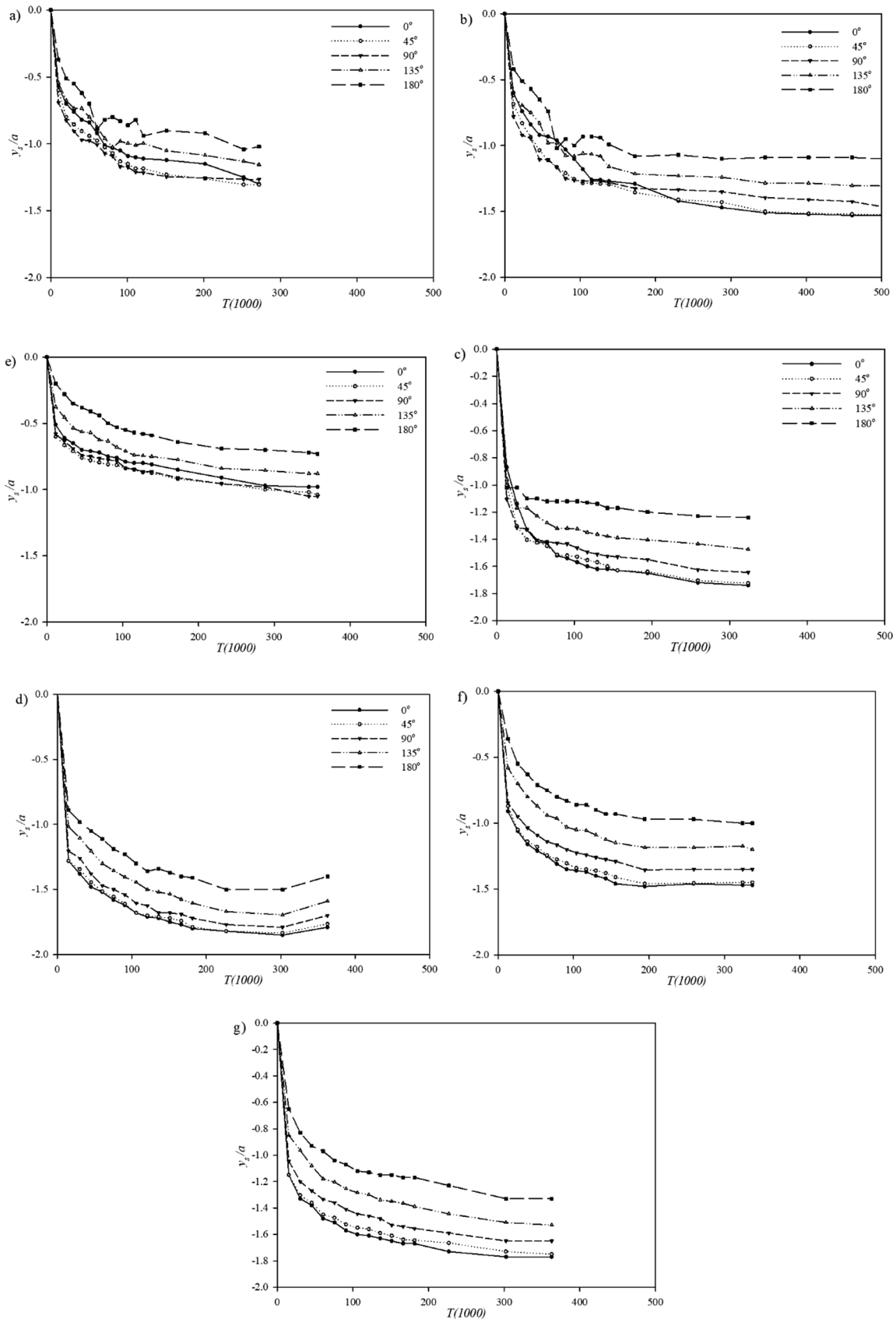


Fig. 4 Temporal scour depth around the pier for sand A and B with 10% cohesive material for **a** Run A101, **b** Run A102, **c** Run A103, **d** Run A104, **e** Run B101, **f** Run B102, **g** Run B103

and $L_s = 1.67 y_{sumax}$. In general, the $L_u \approx 1.5 y_{sumax}$ and $L_s \approx 1.7 y_{sumax}$, irrespective to the pier Reynolds number for $Re_{pi} > 22,000$.

The spatial diagram of ultimate scour hole for sand B with different pier Reynolds numbers is shown in Fig. 5. As can be observed from the data, the location of the sediment settlement at the downstream of the pier (for example 14 cm and 8 cm at downstream for Run A001 and B001, respectively), is more related to the ratio of V/V_c . Increment in V/V_c caused an increase in the distance of sediment settlement from the downstream of pier perimeter. The reason is that higher velocity produces stronger wake vortices which can remain for longer distance at the downstream of the pier. A similar semi ellipsoidal scour hole was also observed for sand B at $Re_{pi} > 24,000$, although increasing Re_{pi} resulted in a horizontal pressed ellipsoid shape due to lower L_u and higher L_s .

3.2 Temporal and Spatial Development of Scour for Cohesive Sands with 10% Cohesive Materials

Experimental Series A10 and B10 were performed to see the temporal and spatial behaviour of scour topography, when 10% cohesive material was added to the sand. The critical velocities (V_c) were determined as 36 and 37 cm/s, for sand-clay mixtures, for A10 and B10 respectively. Figure 4 illustrates the temporal development of local scour for cohesive sand. As can be found from this figure, with increasing the Re_{pi} from 28 to 42 K, the maximum and minimum scour depths increase. In addition, the y_{sumax} occurred at $\alpha = 0^\circ$ or $\alpha = 45^\circ$ while the minimum value occurred in $\alpha = 180^\circ$. For all experiments the highest rate of scour occurred in the first hour of experiments with values of 69–87 mm/h which located at $\alpha = 90^\circ$.

Figure 4 illustrates temporal development of local scour for sand B10 with 10% added cohesive materials (series B10). For sand B at $Re_{pi} = 22,000$ ($V = 22$ cm/s), the maximum rate of scour during the first hour was 24 mm/h at $\alpha = 45^\circ$. Increasing the pier Reynolds number Re_{pi} to 32,000 ($V = 32$ cm/s), however produced an increment in scour rate to 87 mm/h at $\alpha = 0^\circ$ during the first hour of experiment. The maximum scour is usually occurred at the upstream of pier at $\alpha = 0^\circ$ for all Reynolds numbers. Data from the temporal maximum scour graphs, indicate a similar scouring behavior, including the magnitude of scour depth at $\alpha = 0^\circ$ and $\alpha = 45^\circ$, when $V/V_c > 0.88$. Throughout the experiments, the y_{sumin} was consistently found at $\alpha = 180^\circ$. It was also observed for both cohesionless sands that increment in the scour depth caused the rate of scour to decrease with

time, which remained the same, until the scour rate became approximately 0 mm/h.

As a summary, based on the behaviour of temporal and spatial scour for experiments Series A10 and B10, increasing the pier Reynolds number caused an increase in the rate of scour and the maximum ultimate scour depth similar to Series A00 and B00. For higher Re_{pi} , the scour depth and scour rate for $\alpha = 0^\circ$ and 45° produced similar profiles and the y_{sumax} was found at $\alpha = 0^\circ$, but for lower Re_{pi} , the y_{sumax} and scour rate was placed at $\alpha = 45^\circ$ and 90° . Throughout the experiments, the y_{sumin} was consistently found at $\alpha = 180^\circ$. In the first hour of experiment, the highest scour rate occurred at $\alpha = 45^\circ$ and $\alpha = 90^\circ$ for sand A and at $\alpha = 0^\circ$ for sand B except Run B001 which was located at $\alpha = 45^\circ$.

The ultimate scour hole spatial diagram for sand types A and B with different pier Reynolds numbers can be seen in Fig. 5. For $Re_{pi} = 28,000$, the upstream and the side lengths of scour hole reached to 18 cm and 22 cm, which means $L_u = 1.34 y_{sum}$ and $L_s = 1.64 y_{sum}$. Increasing the pier Reynolds number to $Re_{pi} = 32,000$, the upstream length became $L_u = 1.44 y_{sum}$ and $L_s = 1.57 y_{sum}$, whilst at $Re_{pi} = 36,000$, the scour hole has dimensions of $L_u = 1.38 y_{sum}$ and $L_s = 1.61 y_{sum}$.

When $Re_{pi} = 32,000$, the upstream length and the side length of scour hole reached to 14 cm and 16 cm, which shows that $L_u = 1.33 y_{sum}$, $L_s = 1.52 y_{sum}$. By increasing the pier Reynolds number to $Re_{pi} = 36,000$, both the upstream and the side lengths became 22 cm ($L_u = L_s = 1.49 y_{sum}$). At $Re_{pi} = 42,000$, the upstream length and the side length of scour hole were found to be 24 cm and 26 cm, respectively ($L_u = 1.36 y_{sum}$, $L_s = 1.47 y_{sum}$).

3.3 Temporal and Spatial Development of Scour for 20% Cohesive Materials

Experimental Series A20 and B20 were performed to investigate the temporal and spatial behaviour of scour topography by adding 20% cohesive material to the sand. The critical velocity (V_c) was determined as 42 cm/s for both sand-clay mixtures A20 and B20. Figure 6a illustrates the temporal development of local scour when $Re_{pi} = 28$ K ($V/V_c = 0.67$). The y_{sumax} occurred at $\alpha = 90^\circ$ and reached to 7.4 cm while the y_{sumin} took place at $\alpha = 0^\circ$ up to 3.5 cm, which means the ratio of y_{sumin}/y_{sumax} reached to 0.47. The highest rate of scour was found at the first hour at $\alpha = 90^\circ$, at 53 mm/h which means that the developed scour depth has already reached $0.72 y_{sumax}$. At the same time, the lowest scour rate was found only 20 mm/h at $\alpha = 0^\circ$ and reached up to $0.27 y_{sumax}$. The average rates of scour were 13.8 mm/h, 0.9 mm/h, 0.1 mm/h and 0 mm/h for $t = 0-5$, 5–10, 10–15 and 15–25 h, respectively.

Figure 6b presents the temporal development of local scour for series A20 when $Re_{pi} = 32$ K ($V/V_c = 0.76$). In this

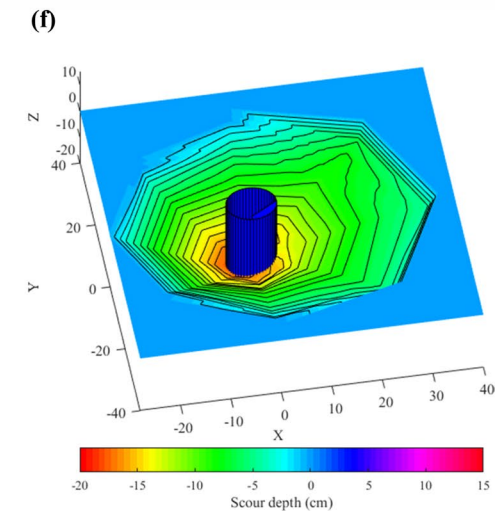
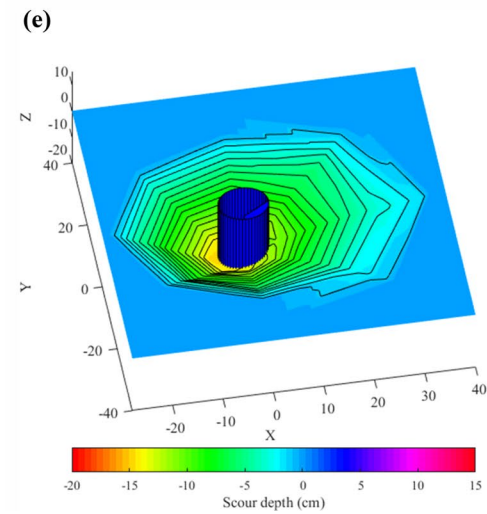
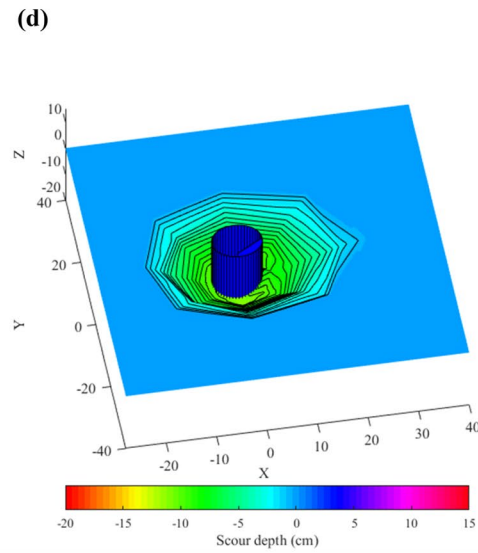
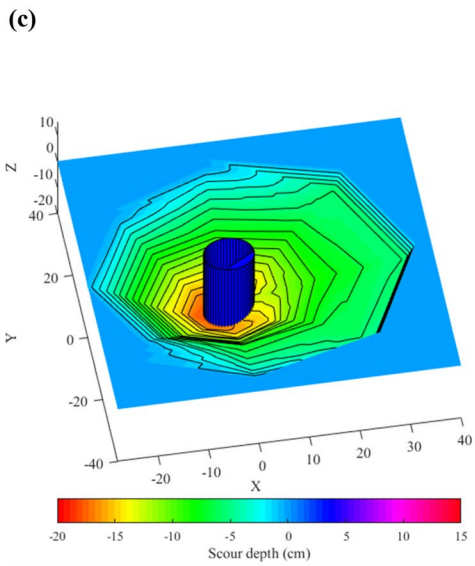
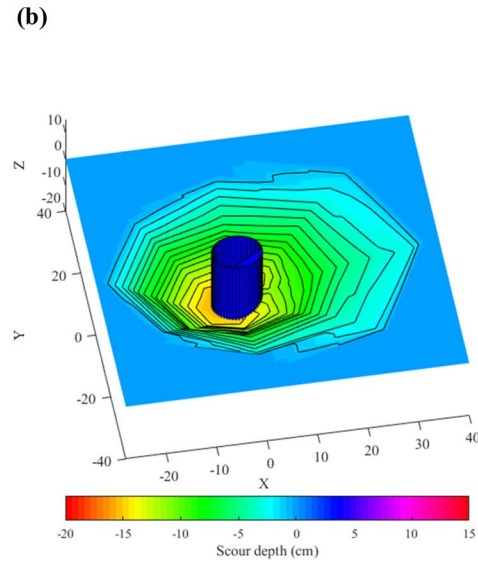
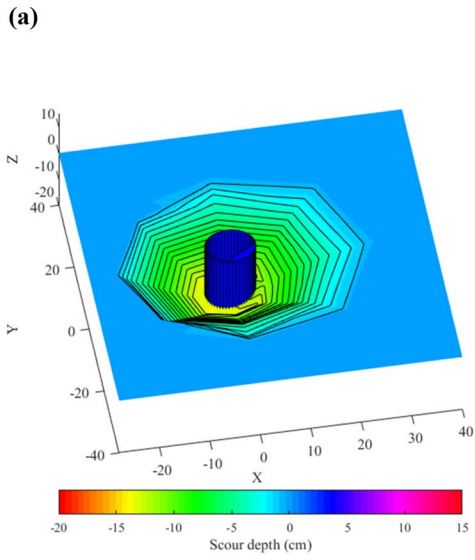


Fig. 5 The spatial characteristics of developed scour hole for sands A and B with 10% cohesive material for **a** Run A101, **b** Run A102, **c** Run A103, **d** Run B101, **e** Run B102, **f** Run B103

case, the y_{sumax} was attained at $\alpha=0^\circ$ and reached to 11.1 cm, whereas the minimum scour rate was achieved at $\alpha=180^\circ$ up to 9.2 cm, which means that at $\alpha=180^\circ$ the ratio of y_{sumin} to y_{sumax} reached up to 0.83. The highest rate of scour was found during the first hour at $\alpha=90^\circ$ with the rate of 79 mm/h (with the developed scour depth of $0.71 y_{sumax}$). Furthermore, during the same time, the minimum scour rate was found at 57 mm/h at $\alpha=180^\circ$ and reached up to $0.51 y_{sumax}$. The average rates of scour were 18.7 mm/h, 2.3 mm/h, 1.2 mm/h and 0 mm/h for $t=0-5$, 5–10, 10–15 and 15–25 h, respectively.

The temporal development of local scour when $Re_{pi}=36K$ ($V/V_c=0.86$) for sand A is shown in Fig. 6c. Here, the y_{sumax} occurred at $\alpha=45^\circ$ and it reached to 16.1 cm, whereas the minimum depth was found at $\alpha=180^\circ$ up to 11.8 cm, which indicates that the ratio of y_{su} at $\alpha=180^\circ$ to y_{sumax} reached to 0.73. The highest rate of scour was found in the first hour at upstream 53 mm/h, located at $\alpha=135^\circ$, with the developed scour depth of almost $0.33 y_{sumax}$. At the same time, the lowest scour rate was found only 33 mm/h at $\alpha=180^\circ$, which resulted in a scour depth of $0.2 y_{sumax}$. The average rates of scour were 23.3 mm/h, 6.3 mm/h, 1.8 mm/h and 0.6 mm/h for $t=0-5$, 5–10, 10–15 and 15–25 h, respectively.

Figure 6c illustrates the temporal development of local scour for sand A when $Re_{pi}=42K$ ($V/V_c=1$). The y_{sumax} took place at $\alpha=0^\circ$ and reaches up to 17.8 cm, while the y_{sumin} was at $\alpha=135^\circ$ and reached up to 14 cm, which implies that $y_{sumin}/y_{sumax}=0.79$. The highest rate of scour was found in the first hour 95 mm/h, located at $\alpha=0^\circ$, with the developed scour depth of $0.53 y_{sumax}$. In addition, during the same time, the lowest scour rate was found only 49 mm/h at $\alpha=180^\circ$ and reached up to $0.28 y_{sumax}$. The average rates of scour were 25.6 mm/h, 3.4 mm/h, 4 mm/h and 1.3 mm/h for $t=0-5$, 5–10, 10–15 and 15–25 h, respectively.

The temporal development of local scour when $Re_{pi}=28K$ for sand B ($V/V_c=0.69$) is presented in Fig. 6d. The y_{sumax} occurred at $\alpha=0^\circ$ and reached to 10.8 cm, while the y_{sumin} was found at $\alpha=45^\circ$ and reached to 9 cm, which means that the ratio of y_{su} to y_{sumax} is 0.83. The highest rate of scour was occurred in the first hour at $\alpha=90^\circ$ with the value of 47 mm/h, which means that the developed scour depth of $0.44 y_{sumax}$. At the same time, the lowest scour rate was found only 26 mm/h at $\alpha=180^\circ$ and reached to $0.24 y_{sumax}$. The average rates of scour were 15.4 mm/h, 0.6 mm/h, 0.8 mm/h and 2.3 mm/h for $t=0-5$, 5–10, 10–15 and 15–25 h, respectively.

The y_{sumax} took place at $\alpha=0^\circ$ and reached up to 13.7 cm for sand B when $Re_{pi}=32K$ ($V/V_c=0.76$) as shown in Fig. 6e. The y_{sumin} was achieved at $\alpha=180^\circ$ that reached up

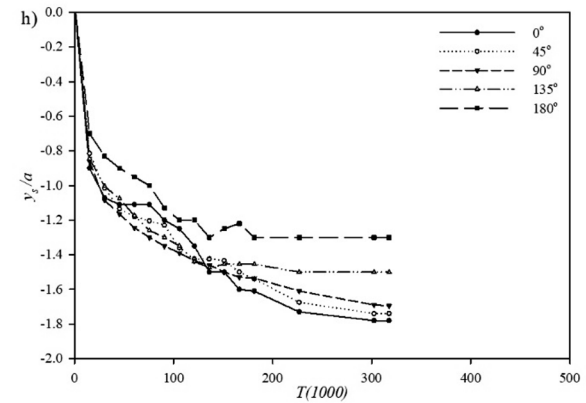
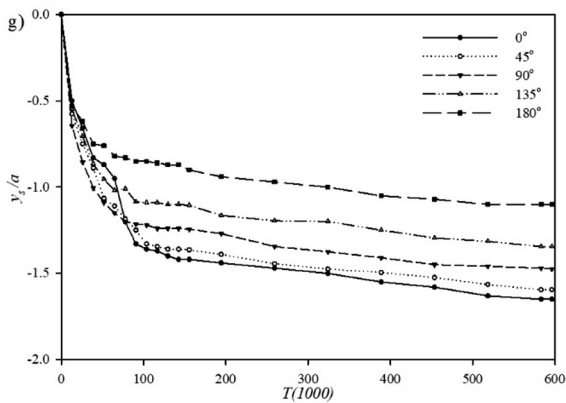
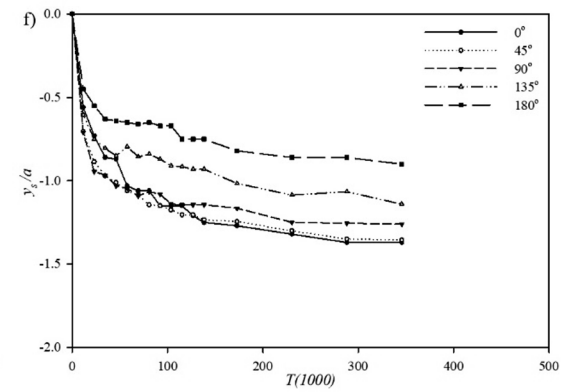
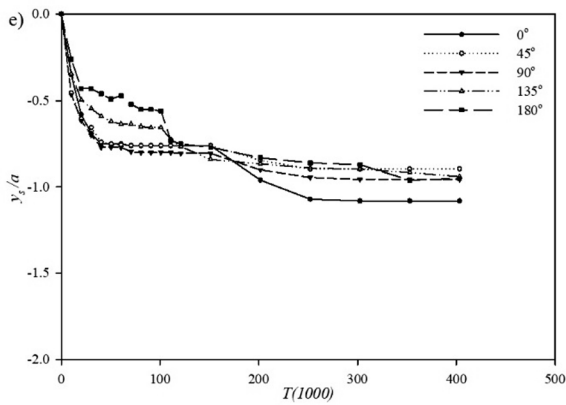
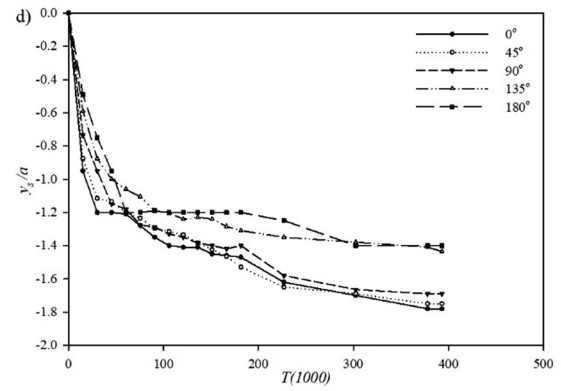
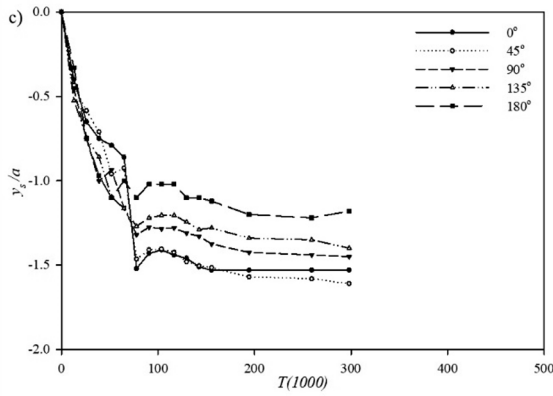
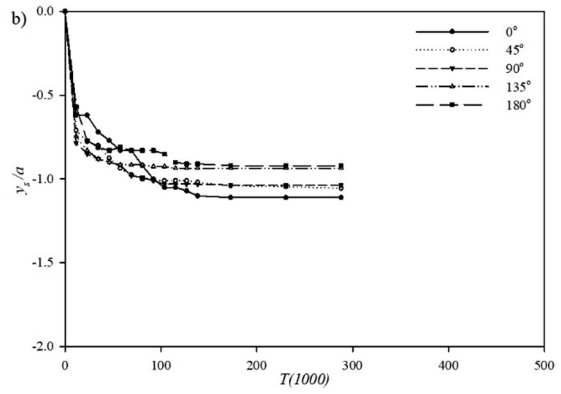
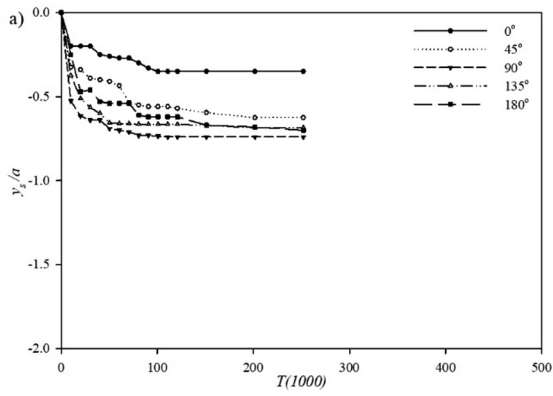
to 9 cm, which denotes that at downstream the ratio of y_{su} at $\alpha=180^\circ$ reached to $0.6 y_{sumax}$. The highest rate of scour happened during the first hour at $\alpha=90^\circ$ with the rate of 78 mm/h, and during this time the scour depth developed up to $0.57 y_{sumax}$. Simultaneously, the lowest scour rate was found only 45 mm/h at $\alpha=180^\circ$ that reached up to $0.33 y_{sumax}$. The average rates of scour were 21.2 mm/h, 2.9 mm/h, 1.3 mm/h and 1 mm/h for $t=0-5$, 5–10, 10–15 and 15–25 h, respectively.

The temporal development of local scour for $Re_{pi}=36K$ ($V/V_c=0.86$) can be seen from Fig. 6f. The maximum ultimate scour depth (y_{sumax}) were found at $\alpha=0^\circ$ that reached up to 16.5 cm, while the y_{sumin} was found at $\alpha=180^\circ$ that reached up to 11 cm. This means that the ratio of y_{su} at $\alpha=180^\circ$ to y_{sumax} reached to 0.67. The highest rate of scour can be found at the first hour in the upstream is 65 mm/h, located at $\alpha=90^\circ$, with the developed scour depth of $0.39 y_{sumax}$. During the same time, the lowest scour rate was found to be 50 mm/h at $\alpha=0^\circ$ that reached up to $0.3 y_{sumax}$. The average rates of scour were 23 mm/h, 5 mm/h, 0.8 mm/h and 0.6 mm/h for $t=0-5$, 5–10, 10–15 and 15–25 h respectively.

Figure 6g illustrates the temporal development of local scour for sand B when $Re_{pi}=42K$ ($V/V_c=1$). At this velocity, the y_{sumax} was seen at $\alpha=0^\circ$ and reached up to 17.8 cm, whilst the y_{sumin} took place at $\alpha=180^\circ$ and reached up to 13 cm, which indicates that at $\alpha=180^\circ$, the ratio of y_{su} to y_{sumax} reached to 0.73. The highest rate of scour was observed in the first hour at upstream 90 mm/h located at $\alpha=0^\circ$, with the developed scour depth of almost $0.51 y_{sumax}$. Simultaneously, the lowest scour rate was only 70 mm/h at $\alpha=180^\circ$ that reached up to $0.39 y_{sumax}$. The average rates of scour were 27 mm/h, 4 mm/h, 4.6 mm/h and 0.5 mm/h for $t=0-5$, 5–10, 10–15 and 15–25 h, respectively.

The ultimate scour hole spatial diagram for sand A with different Reynolds numbers are presented in Fig. 7. When $Re_{pi}=32,000$, the upstream length and the side length of scour hole reached to 12 cm and 16 cm, which are $1.08 y_{sumax}$ and $1.44 y_{sumax}$ respectively. While the pier Reynolds number increased to $Re_{pi}=36,000$, the upstream length became 16 cm and the side length became 20 cm ($L_u=0.99 y_{sumax}$, $L_s=1.24 y_{sumax}$). At $Re_{pi}=42,000$, the upstream length and the side length of scour hole were found to be 22 cm and 26 cm respectively ($L_u=1.24 y_{sumax}$, $L_s=1.46 y_{sumax}$).

The upstream length and the side length of scour hole reached to 12 cm and 16 cm respectively ($L_u=1.11 y_{sumax}$, $L_s=1.48 y_{sumax}$), when $Re_{pi}=28,000$. As the pier Reynolds number increased to $Re_{pi}=32,000$, both the upstream and the side lengths were expanded to be 16 cm became 22 cm, respectively giving relation to the y_{sumax} as 1.17 and 1.61. At $Re_{pi}=36,000$, the upstream length and the side length of scour hole were found to be 16 cm and 24 cm respectively ($L_u=0.97 y_{sumax}$, $L_s=1.45 y_{sumax}$). Whereas, the value of



◀**Fig. 6** Temporal scour depth around the pier for sand A and B with 10% cohesive material for **a** Run A201, **b** Run A202, **c** Run A203, **d** Run A204, **e** Run B201, **f** Run B202, **g** Run B203, **h** Run B204

upstream and side lengths at $Re_{pi}=42,000$ are 20 cm and 26 cm respectively ($L_u = 1.12 y_{sumax}$, $L_s = 1.46 y_{sumax}$).

3.4 Temporal and Spatial Development of Scour for 30% Cohesive Materials

The last series of experiments were conducted to uncover the temporal and spatial behaviour of scour topography by adding 30% cohesive material to sand A and B. Due to the existing pump capacity, it was not permissible to conduct the experiments with $V/V_c > 0.86$. However, successfully conducted experiments under $V/V_c \leq 0.86$ provide insightful knowledge on how high percentage of cohesive material influence the scour profile.

Figure 8a illustrates temporal development of local scour for sand A30 when $Re_{pi} = 36K$ ($V/V_c = 0.73$). The y_{sumax} of 9.8 cm occurred at $\alpha = 135^\circ$, while the y_{sumin} of 2.1 cm was found at $\alpha = 0^\circ$. Thus, the ratio of y_{su} at $\alpha = 0^\circ$ to y_{sumax} gives value of 0.21. The highest rate of scour was observed in the first hour at the upstream, with the scour rate of 25 mm/h at $\alpha = 135^\circ$, with the developed scour depth of $0.26 y_{sumax}$. At the same time, the lowest scour rate was found to be only 0 mm/h at $\alpha = 0^\circ$. The average rates of scour were 13.6 mm/h, 3.8 mm/h, 0 mm/h and 1.1 mm/h for $t = 0-5$, $5-10$, $10-15$ and $15-25$ h, respectively.

The maximum scour depth (y_{sumax}) for sand A with 30% added cohesive material, when $Re_{pi} = 42K$ ($V/V_c = 0.86$) occurred at $\alpha = 90^\circ$ and reached to 12.9 cm as shown in Fig. 8b. The y_{sumin} was found at $\alpha = 135^\circ$ up to 11.7 cm, which means that the ratio of y_{su} at $\alpha = 135^\circ$ to y_{sumax} gives the value of 0.91. The highest rate of scour was found at the first hour at $\alpha = 135^\circ$ which reached to 37 mm/h, with the developed scour depth found at $0.28 y_{sumax}$. At the same time, the lowest scour rate was found only 23 mm/h located at $\alpha = 180^\circ$ and the scour depth reached up to $0.18 y_{sumax}$. The average rates of scour were 20 mm/h, 4.2 mm/h, 1.5 mm/h and 0 mm/h for $t = 0-5$, $5-10$, $10-15$ and $15-25$ h respectively.

The temporal development of local scour for sand B with 30% cohesive material for $Re_{pi} = 36K$ ($V/V_c = 0.73$) is shown in Fig. 8c. The y_{sumax} was found at $\alpha = 135^\circ$ and reached to 7.6 cm while the minimum was at $\alpha = 0^\circ$ with 1.5 cm scour depth. This brings the ratio of y_{su} at $\alpha = 0^\circ$ to y_{sumax} was 0.20. The highest rate of scour was found at $\alpha = 90^\circ$ during the first hour of experiment with 43 mm/h scour rate at, thus the developed scour depth gives $0.57 y_{sumax}$. At the same time, the minimum scour rate was found only 10 mm/h at $\alpha = 0^\circ$ and reached up to $0.13 y_{sumax}$. The average rates of

scour were 12 mm/h, 1.7 mm/h, 0.8 mm/h and 0.2 mm/h for $t = 0-5$, $5-10$, $10-15$ and $15-25$ h, respectively.

Figure 8d demonstrates the temporal development of local scour when $Re_{pi} = 42K$ (i.e. $V/V_c = 0.86$) for sand B with 30% cohesive material. The y_{sumax} was found at $\alpha = 180^\circ$ and reached to 7.9 cm while the minimum was at $\alpha = 0^\circ$ up to 1.8 cm, which means the ratio of y_{su} at this location to y_{sumax} reached to 0.23. The highest rate of scour was found at the first hour at the upstream where the location is $\alpha = 90^\circ$, with the value of 65 mm/h and the developed scour depth of $0.82 y_{sumax}$. At the same time, the lowest scour rate was found 18 mm/h at $\alpha = 0^\circ$ and the bed material was scoured up to $0.23 y_{sumax}$. The average rates of scour were 15.1 mm/h, 0.5 mm/h, 0.2 mm/h and 0 mm/h for $t = 0-5$, $5-10$, $10-15$ and $15-25$ h respectively.

As shown in Fig. 8, scour profiles around pier, when high percentage (30%) of cohesive material was added to the sediment mixtures, the opposite scour profiles were obtained comparing to sediment mixtures with low percentages of cohesive materials. While for cohesionless sediment the maximum ultimate scour depth consistently was at the upstream located at $\alpha = 0^\circ$ and 45° and the minimum was found to be consistently at $\alpha = 180^\circ$, for the cohesive sediment with 30% of cohesive material the location of maximum and y_{sumin} was found to be even opposite of the cohesionless sediment mixtures. The minimum ultimate scour depth was consistently placed at $\alpha = 0^\circ$, while the maximum was placed at $\alpha = 90^\circ$, 135° and 180° .

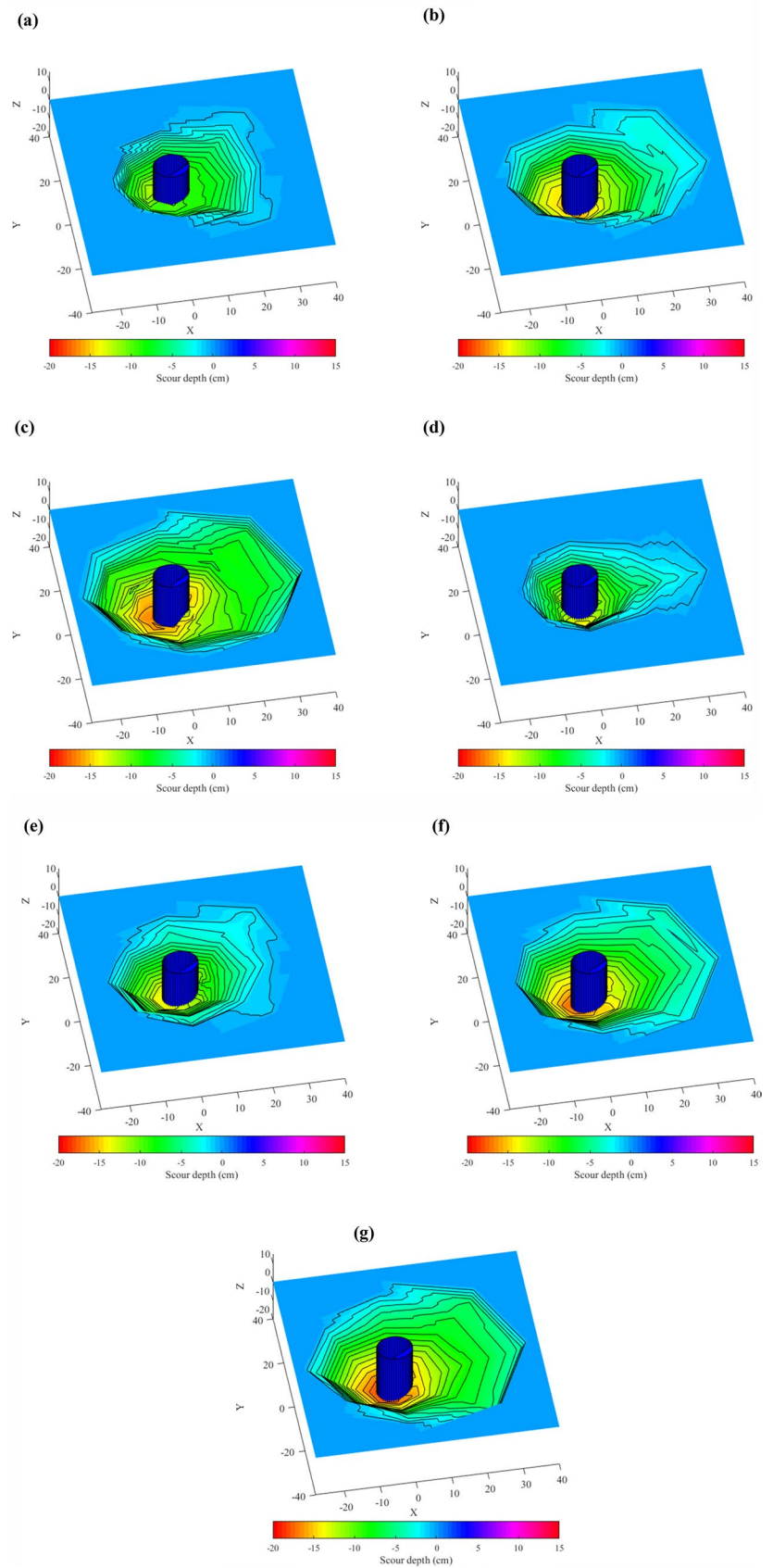
Figure 9 presents the ultimate scour hole spatial diagram for sand A with different Reynolds numbers. When $Re_{pi} = 36,000$, the upstream and the side lengths of scour hole reached to 12 cm and 14 cm respectively ($L_u = 1.22 y_{sumax}$, $L_s = 1.43 y_{sumax}$). Whereas, when the pier Reynolds number was increased to $Re_{pi} = 42,000$, the ratio of lengths to the maximum ultimate scour depth were $L_u/y_{sumax} = 1.52$, $L_s/y_{sumax} = 1.71$, respectively.

The ultimate scour hole spatial diagrams for sand B with different Reynolds numbers are illustrated in Fig. 9. When $Re_{pi} = 36,000$, the upstream length and the side length of scour hole reached to 4 cm and 8 cm respectively ($L_u = 0.53 y_{sumax}$, $L_s = 1.05 y_{sumax}$). While the pier Reynolds number was increased to $Re_{pi} = 42,000$, the developed upstream and the side lengths were equal to 10 cm, resulted similar L_u/y_{sumax} and L_s/y_{sumax} at 1.

4 Discussion

The developed ADRS allows for a scrutiny spatial–temporal assessment on the progress of scour around bridge piers in clay–sand mixed beds, from initiation until equilibrium. The summary of dataset for all experiments is shown in Table 2. To assist in the discussion, we denote the region

Fig. 7 The spatial characteristics of developed scour hole for sand A and B with 20% cohesive material for **a** Run A202, **b** Run A203, **c** Run A204, **d** Run B201, **e** Run B202, **f** Run B203, **g** Run B204



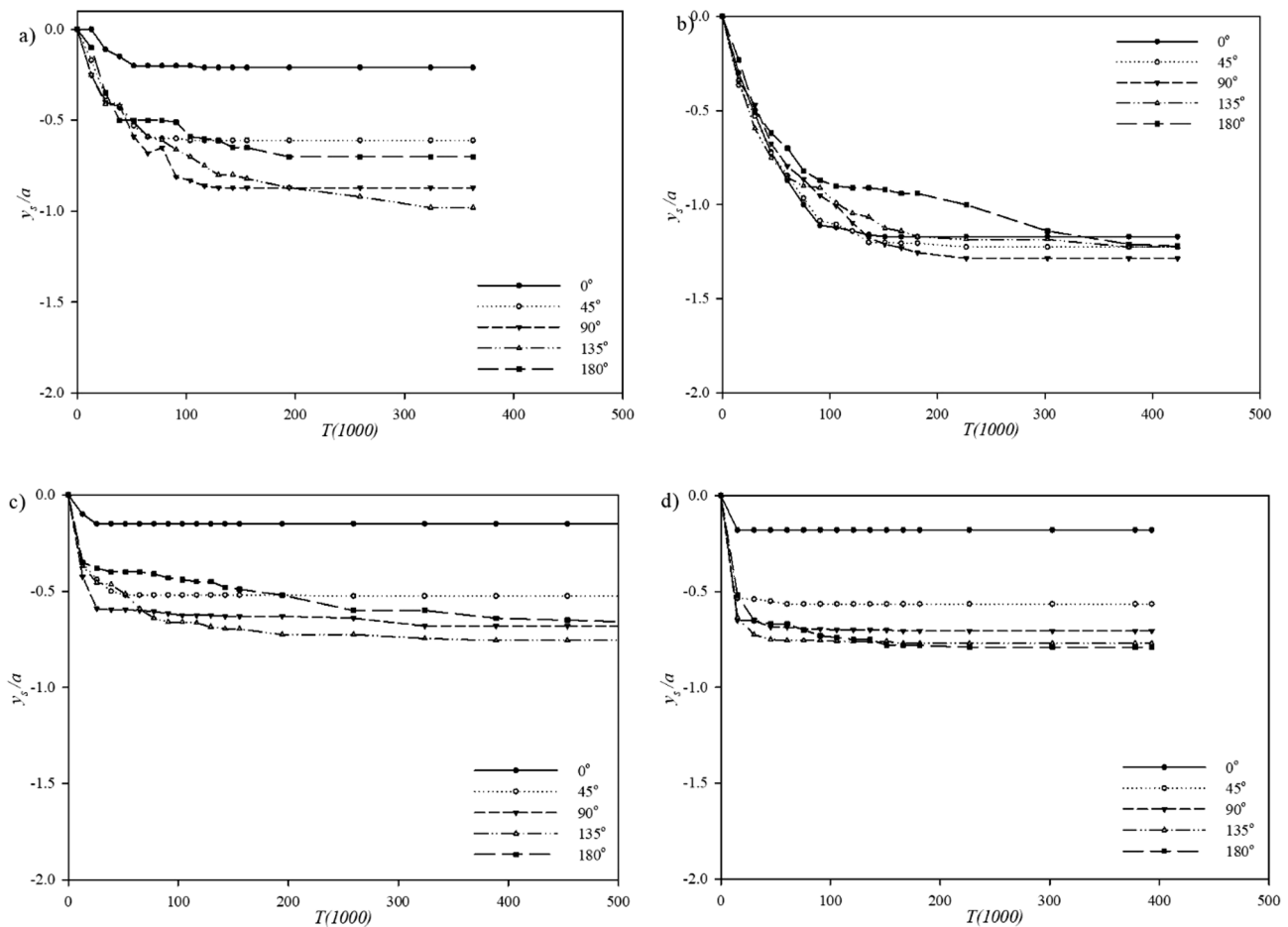


Fig. 8 Temporal scour depth around the pier for sand B with 20% cohesive material for **a** Run A301, **b** Run A302, **c** Run B301, and **d** Run B302

from 0° to 90° as upstream midline and 90° – 180° as downstream midline. The presence of cohesive material in the sand bed influences the scour development even with additional of 10% and becomes more apparent with higher fractions. In general, the scour was initiated with active bed movement was observed throughout the peripheral of the pier. Passing the early stage of scouring, visual observation showed inactive bed movement, but continuous scouring was evident based on the temporal measurement of scour depth. The location of y_{sumax} however, varied with time, depending on Re_{pi} and percentage of clay C . At low Re_{pi} and clay fraction of 10%, side scouring was dominant at the upstream midline regions at the early stage. The scouring was initiated at the wake and sides of the pier owing to the high capacity of entrainment, with 11 times shear stress more than the approach flow (Kumar and Kothiyari 2012), whereas the shear stress at the pier nose is about four times more (Ahmad and Rajaratnam 1998). As the scouring reaching the advanced stages, the maximum location progressively moves towards the upstream of the pier. The strength of downflow increases as the size

and strength of the vortex increase when the scour hole enlarges (Ali and Karim 2000).

Increasing clay fraction to 20% provide a different scenario where scouring was rigorous in the downstream midline region and progressive move towards the midline over time. The scouring was dominant at the downstream midline, with deeper scour depth was observed for sediment bed with 30% of clay. The impact from the wake vortices and horseshoe vortex were although did not cause instantaneous erosion, it was believed to slowly disrupt the forces between the agglomeration of clay-sand and collapsed once it loses the integration, providing rugged surface of scour hole. The resistance to erosion as the net inter-particle surface force increases with increasing percentage of clay (Rambabu et al. 2003). The dominant mode of sediment removal is chunks of aggregate.

Increasing Re_{pi} (that is increasing V/V_c) provide prevalent side scouring at the upstream and downstream midlines for C of 10% and 20%, respectively, before the downflow becomes significant eroding the bed material at the later stage of scouring. At $C=30\%$, downflow and horseshoe

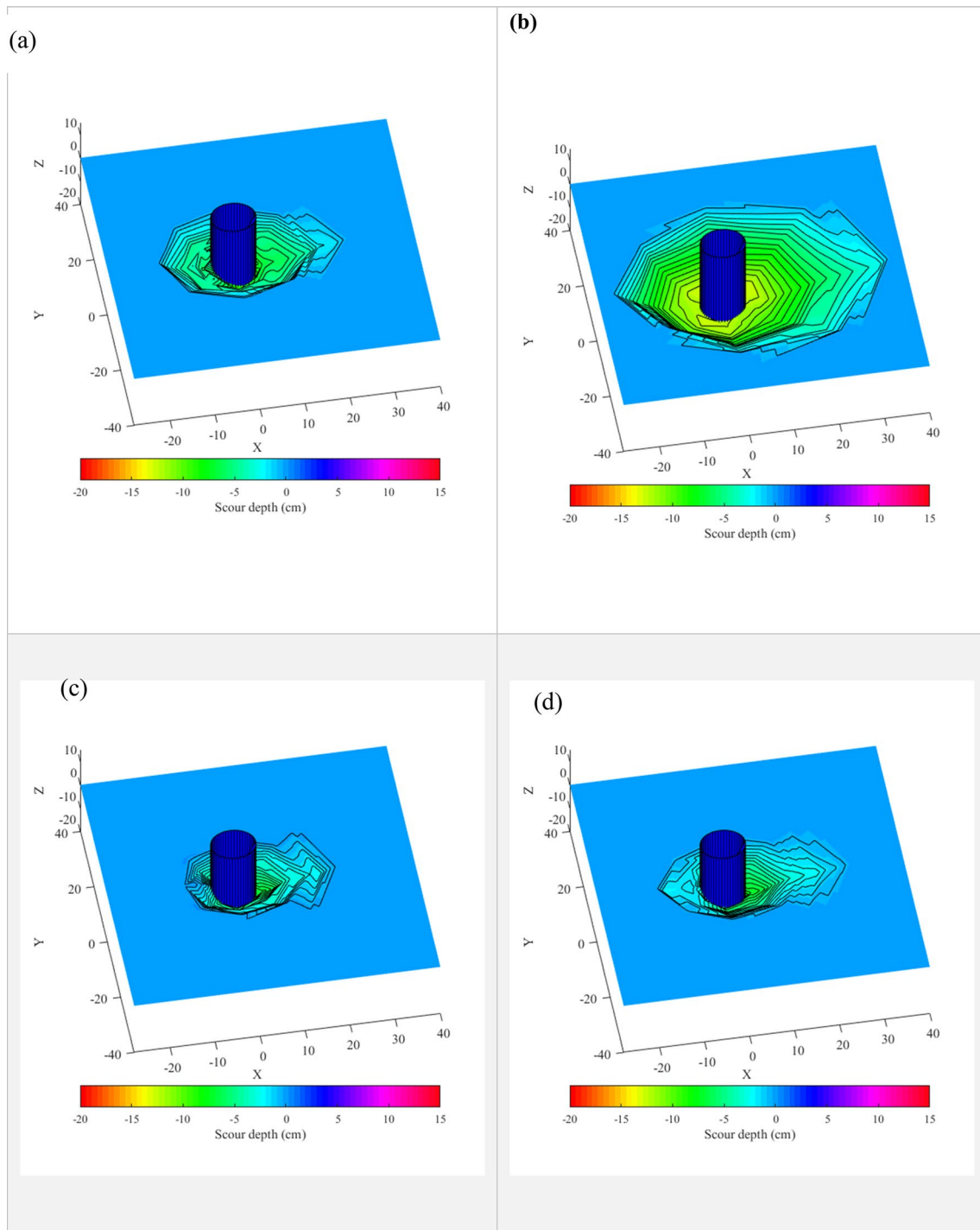


Fig. 9 The spatial characteristics of developed scour hole for sand A with 30% cohesive material for **a** Run A301, **b** Run A302, **c** Run B301, **d** Run B302

vortex were both dominant entraining the sediment bed at the early stage, where the scour depth remains stationary before sharp decrease to reaching quasi-equilibrium. It is believed that abrupt erosion when chunks of sand-clay aggregate lose its adjacent forces and disintegrate with the surrounding bed. The rough cohesive surface distorts the

formation of fully developed horseshoe vortex, diminishing the continuous erosivity power like in the smooth non-cohesive bed (Chaudhuri and Debnath 2013). We use the term quasi-equilibrium as scouring in cohesive soil (or cohesive like sediment) proved to be a long affair and may be exponentially predicted (Molinas and Hosny 1999; Debnath

and Chaudhuri 2010). Different scenario was observed for Sand B with downstream midline scouring was significant throughout (and even reached to downstream of the pier at 180°). Similar finding where the scour propagates gradually towards the downstream of the pier was observed for high percentage of clay bed ($> 35\%$) and high Re_{pi} (Chaudhuri and Debnath 2013) and 100% clay bed (Briaud et al. 1999; Ting et al. 2001).

Increase in clay content showed steeper slopes for scour holes (Molinas and Hosny 1999) and this study showed that holds even for clay-sand mixture with coarser sand size. Experiments with high C and even more at high Re_{pi} , produced high turbidity throughout the experimental runs, due to the transportation of suspended particle of eroded bed material. At this velocity, the mechanism of sediment removal is chunk of aggregate (and break up whilst in suspension) and particle-by-particle.

We observed similar y_{sumax} and quasi-equilibrium scour pattern (except for B3 series experiments) with non-cohesive experiments, believed to be due to low antecedent moisture content and unsaturated soil condition. Combination of shearing resistance of clay-sand bed and the generated shear stress from the flow determines the location of the maximum scour depth (Debnath and Chaudhuri 2010). In a mixture with 30% clay, the sand sediment size plays an important role in the scour hole shape, where the bed material with coarser sand has lower erosivity compared to the mixture with smaller sand size. The scouring at the downstream of pier is prominent than the upstream location (as shown in Fig. 9). Coarser sediment size performs stronger inter-particle surface force with the cohesive material, giving higher resistance to be entrained. As this study use kaolinite as clay material, it is envisaged that where dominant clay mineral is illite or montmorillonite, the scour area is smaller due to high cohesion (Devi and Barbhuiya 2017).

5 Conclusion

Most of the natural sediments in the rivers contain some percentage of cohesive sediment such as clay, which changes the characteristics of the incipient motion of sediments due to their interparticle forces. In present study, an experimental setup was conducted to measure the rate of scour depth in both cohesionless and cohesive sediment with three different percentages of clay ranging from 0 to 30%. A low-cost automated data recording system (ADRS) controlled by Arduino microcontroller was designed and developed to obtain spatial and temporal data in different time intervals.

Based the results, for both cohesionless sand types, at the initial stage (i.e., the first hour of experiment), the scour depth reached to $\approx 50\%$ of the maximum ultimate scour depth. Increasing the velocity (and the associated Re_{pi})

caused a higher rate of scour at the initial stage. However, the scour rate was significantly reduced with the development of the scour in the middle stage until it got nearly to the value smaller than D_{50}/hour at the final stage. Increasing V/V_c caused an increment in the ratio of minimum to maximum scour depth (y_{sumin}/y_{sumax}) for cohesionless sediment mixtures, which resulted in a more uniform peripheral scour. For sand-clay sediment mixtures with up to 20% cohesive materials, $y_{sumin}/y_{sumax} \approx 0.7$. However, by adding 30% of cohesive materials, the ratio of y_{sumin}/y_{sumax} became significantly lower to 0.2. The side length of scour hole was observed to have higher value than the upstream length for all experiments. This study showed that the influence of cohesive material becomes significant for 30% clay fractions, where less cohesive fractions exhibit similar scour profile to the non-cohesive sediment. Even so, the effect of cohesion becomes critical for temporal scour characterisation and the determination of critical velocity.

This study provides a detailed description on how the peripheral scour around cylindrical pier in varying cohesive material. As the shape of bridge pier is not essentially cylindrical, the effect of pier shape and installation of scour countermeasure (for example riprap, collar) on the local scour profile would allow a better understanding on the influence of cohesive material in scouring process.

Acknowledgements The authors express gratitude for the financial support given by the Ministry of Education through ERGS/1/2013/TK03/UKM/02/7 and Universiti Kebangsaan Malaysia under the Grant DPK-2020-006.

References

- Ahmed F, Rajaratnam N (1998) Flow around bridge piers. *J Hyd Eng ASCE* 124(3):288–299
- Akib S, Othman F, Sholichin M, Fayyadh MM, Shirazi SM, Primasari B (2011) Influence of flow shallowness on scour depth at semi-integral bridge piers. *Adv Mater Res* 243–249:4478–4481
- Ali KHM, Karim O (2000) Simulation of flow around piers. *J Hydraul Res* 40(2):161–174
- Ansari SA, Kothiyari UC, Ranga Raju KG (2002) Influence of cohesion on scour around bridge piers. *J Hydraul Res* 40:717–729
- Arneson LA, Zevenbergen LW, Lagasse PF, Clopper PE (2012) Evaluating scour at bridges Fifth Edition. U.S. Department of Transportation, Washington, D.C. Retrieved from <http://www.fhwa.dot.gov/engineering/hydraulics/pubs/hif12003.pdf>
- Brandimarte L, Paron P, Di Baldassarre G (2012) Bridge pier scour: a review of processes, measurements and estimates. *Environ Eng Manag J* 11:975–989
- Briaud J-L, Ting FCK, Chen HC, Gudavalli R, Perugu S, Wei G (1999) SRICOS: prediction of scour rate in cohesive soils at bridge piers. *J Geotech Geoenviron Eng ASCE* 125(4):237–246
- Chaudhuri S, Debnath K (2013) Observations on initiation of pier scour and equilibrium scour hole profiles in cohesive sediments. *ISH J Hydraul Eng* 19(1):27–37
- Chaudhuri S, Singh SK, Debnath K, Manik MK (2018) Pier scour within long contraction in cohesive sediment bed. *Environ Fluid Mech* 18:417–441

- Chiew YM (1984) Local scour at bridge piers. PhD thesis. Auckland University
- Das VK, Chaudhuri S, Barman K, Roy S, Debnath K (2020) Pier scours in fine-grained non-cohesive sediment and downstream siltation, an experimental approach. *Phys Geogr*. <https://doi.org/10.1080/02723646.2020.1801372>
- Debnath K, Chaudhuri S (2010) Laboratory experiments on local scour around cylinder for clay and clay–sand mixed bed. *Elsevier Eng Geol* 111(12):51–61
- Debnath K, Chaudhuri S (2011) Effect of suspended sediment concentration on local scour around cylinder for clay–sand mixed sediment beds. *Eng Geol* 117:236–245
- Devi YS, Barbhuiya AK (2017) Bridge pier scour in cohesive soil: a review. *Sādhanā* 42(10):1803–1819
- Dey S, Barbhuiya AK (2004) Clear-water scour at abutments in thinly armored beds. *J Hydraul Eng* 130:622–634
- Dumas C, Krolack J (2002) A geotechnical perspective: design and construction of highway bridge foundations for scour. In: *Proceedings of the first international conference on scour of foundations*, Texas A&M University, College Station, USA, pp 112–119
- Hjulström F (1935) Studies of the morphological activity of rivers as illustrated by the River Fyris. *Bull Geol Inst Upsala* 25:221–527
- Hosseinjanzadeh H, Sheikh Khozani Z, Ardeshir A, Singh VP (2019) Experimental investigation into the use of collar for reducing scouring around short abutments. *ISH J Hydraul Eng*:1–17
- Khosravi K, Khozani ZS, Mao L (2021) A comparison between advanced hybrid machine learning algorithms and empirical equations applied to abutment scour depth prediction. *J Hydrol* 596:126100
- Kothyari UC, Garde RCJ, Ranga Raju KG (1992) Temporal variation of scour around circular bridge piers. *J Hydraul Eng* 118:1091–1106
- Kumar A, Kothyari UC (2012) Three-dimensional flow characteristics within the scour hole around circular uniform and compound piers. *J Hydraul Eng* 138(5):420–429
- Link O, Pflieger F, Zanke U (2008) Characteristics of developing scour-holes at a sand-embedded cylinder. *Int J Sediment Res* 23:258–266
- Link O, Klischies K, Montalva G, Dey S (2013) Effects of bed compaction on scour at piers in sand-clay mixtures. *J Hydraul Eng* 139:1013–1019
- Mazumder SK (2017) Scour in bridge piers on non-cohesive fine and coarse soil. *ISH J Hydraul Eng* 23:111–117
- Melville BW (1975) Local scour at bridge sites. University of Auckland
- Melville BW, Chiew Y (1999) Time scale for local scour at bridge piers. *J Hydraul Eng* 125:59–65
- Molinas A, Hosny MM (1999) Effect of gradations and cohesion on bridge scour. vol. 4. *Experimental study of scour around Circular Piers in Cohesive soils*. FHWA-RD-99-186
- Najafzadeh M, Lim SY (2015) Application of improved neuro-fuzzy GMDH to predict scour depth at sluice gates. *Earth Sci Inform* 8:187–196
- Namaee MR, Sui J (2019) Impact of armour layer on the depth of scour hole around side-by-side bridge piers under ice-covered flow condition. *J Hydrol Hydromech* 67:240–251
- Partheniades E (2009) *Cohesive sediments in open channels : properties, transport, and applications*. Butterworth-Heinemann/Elsevier, p 358
- Porhemmat M, Wan Mohtar WHM, Chuah RE, Abd Jalil J (2016) The comparison of empirical formula to predict the incipient motion of weak cohesive sediment mixture. *J Teknol* 78:109–114
- Rambabu M, Narasimha RS (2003) Current induced scour around a vertical pile in cohesive soil. *Ocean Eng* 30(4):893–920
- Singh RK, Pandey M, Pu JH, Pasupuleti S, Villuri VGK (2020) Experimental study of clear-water contraction scour. *Water Supply* 20:943–952
- Ting FCK, Briaud J-L, Chen HC, Gudavalli R, Perugu S, Wei G (2001) Flume tests for scour in clay at circular piers. *J Hydraul Eng* 127:969–978
- Yang Y, Melville BW, Macky GH, Shamseldin AY (2020) Experimental study on local scour at complex bridge pier under combined waves and current. *Coast Eng* 160:103730

Springer Nature or its licensor (e.g. a society or other partner) holds exclusive rights to this article under a publishing agreement with the author(s) or other rightsholder(s); author self-archiving of the accepted manuscript version of this article is solely governed by the terms of such publishing agreement and applicable law.